

Alma Mater Studiorum Università di Bologna  
Archivio istituzionale della ricerca

Force-Distribution Sensitivity to Cable-Tension Errors: A Preliminary Investigation

This is the final peer-reviewed author's accepted manuscript (postprint) of the following publication:

*Published Version:*

Mattioni V., Ida E., Carricato M. (2021). Force-Distribution Sensitivity to Cable-Tension Errors: A Preliminary Investigation. Cham : Springer Science and Business Media B.V. [10.1007/978-3-030-75789-2\_11].

*Availability:*

This version is available at: <https://hdl.handle.net/11585/826615> since: 2021-07-02

*Published:*

DOI: [http://doi.org/10.1007/978-3-030-75789-2\\_11](http://doi.org/10.1007/978-3-030-75789-2_11)

*Terms of use:*

Some rights reserved. The terms and conditions for the reuse of this version of the manuscript are specified in the publishing policy. For all terms of use and more information see the publisher's website.

This item was downloaded from IRIS Università di Bologna (<https://cris.unibo.it/>).  
When citing, please refer to the published version.

(Article begins on next page)

This is the final peer-reviewed accepted manuscript of:

Mattioni, V., Idà, E., Carricato, M.

Force-Distribution Sensitivity to Cable-Tension Errors: A Preliminary Investigation

In:

*Gouttefarde, M., Bruckmann, T., Pott, A. (eds) Cable-Driven Parallel Robots. CableCon 2021. Mechanisms and Machine Science, vol 104. Springer, Cham.*

The final published version is available online at:

[https://doi.org/10.1007/978-3-030-75789-2\\_11](https://doi.org/10.1007/978-3-030-75789-2_11)

Rights / License:

The terms and conditions for the reuse of this version of the manuscript are specified in the publishing policy. For all terms of use and more information see the publisher's website.

*This item was downloaded from IRIS Università di Bologna (<https://cris.unibo.it/>)*

***When citing, please refer to the published version.***

# Force-Distribution Sensitivity to Cable-Tension Errors: A Preliminary Investigation

Valentina Mattioni<sup>[0000-0002-5505-8731]</sup>, Edoardo Idà<sup>[0000-0003-0437-4651]</sup>,  
Marco Carricato<sup>[0000-0002-1528-4304]</sup>

University of Bologna, Department of Industrial Engineering, Bologna, Italy  
{valentina.mattioni, edoardo.ida2, marco.carricato}@unibo.it

<http://www.irmalab.org/>

**Abstract.** In order to control cable-driven parallel robots (*CDPRs*), it is necessary to keep all cable tensions within (positive) known limits during motion. For *CDPRs* having more cables than end-effector degrees of freedom, a feasible force distribution within cables should be computed beforehand. This paper aims at evaluating how a tension error in one cable affects the overall distribution of tensions in the other cables, by focusing on planar overconstrained *CDPRs* with four cables. The cable whose tension error more limitedly impact the force distribution is analytically determined by computing the right nullspace of the manipulator structure matrix. It is then shown how the cable least influencing the force distribution changes throughout the wrench-feasible workspace. Lastly, the results of the proposed analysis are used to perform a motion-control experiment on a prototype, where, for any configuration of the end-effector, the cable least influencing the force distribution is tension-controlled, while the remaining ones are length-controlled.

**Keywords:** Overconstrained cable-driven parallel robots, Force distribution, Workspace computation.

## 1 Introduction

A parallel robot, whose rigid links are replaced by flexible cables, is known as a Cable Driven Parallel Robot (*CDPR*). Cables are coiled and uncoiled by motorized winches, usually placed on a fixed base, and drive the end-effector (*EE*) throughout its workspace (*WS*). The use of light cables, instead of rigid links, brings numerous advantages in term of *WS* dimension, dynamic performances, payload capability and robot cost. These features make *CDPRs* suitable for a variety of applications in the field of logistics [1], construction [2, 3] and pick and place [4], just to name a few. *CDPRs* control is complicated by the fact that cables can only exert tensile forces, thus, they cannot generate wrenches in every direction [5]. To overcome this issue, usually they include more actuated cables than those that are strictly needed to control the platform pose, with cables pulling one against the other. Overconstrained *CDPRs* (*OCDPRs*) require special control techniques, usually based on the closed-loop control of cable tensions between a minimum and a maximum value. Cable-force values can be computed by solving the static equations for a given pose of the *EE*,

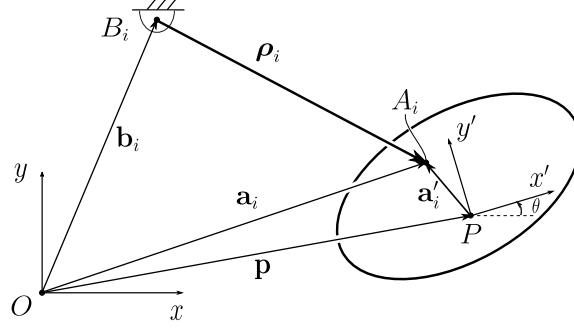
and employed for the determination of torque set-points for the actuators. However, under the assumption of inextensible cables, the static-equilibrium problem for an overconstrained system is underdetermined, thus admitting an infinite number of solutions for every *EE* pose. This makes the determination of cable forces non-trivial. This problem is known in the literature as Force or Tension Distribution (*FD*) computation. *FD* computation can be formulated as an optimization problem [6], or, if real-time capability is an application requirement [7], methods with less computation complexity, such as geometrical approaches, can be used [8,9].

The aim of this work is to evaluate how *FD* varies with respect to an error in the force of one cable, and to determine which cable-tension error influences the least the *FD*. In other words, the *FD* sensitivity to one cable tension error is evaluated and the cable whose tension error results in the minimum *FD* sensitivity is identified. Then, the wrench-feasible workspace of a planar *OCDPR* with two different cable arrangements is computed, according to a well-known kernel-based approach, and it is shown that the cable least influencing the *FD* varies in the *WS*. The identification of this cable is then used for the preliminary test of a hybrid-input control strategy of a 4-cable 3-*DoF* *CDPR*. This strategy, introduced in [10] and [11], requires that three cables, equal to the number of platform *DoFs*, are length-controlled, whereas the redundant cable is force-controlled. This simple feedforward control scheme provides a good *EE* motion accuracy, while it succeeds in maintaining all cables taut throughout the *WS*, without requiring more involved cascade closed-loop controllers [12]. References [10] and [11] suggest no procedure for the selection of the force-controlled cable, while, in this paper, it is determined by way of the results of sensitivity analysis. The aim is to ensure that the *FD* error is kept as low as possible, while preserving the *WS* dimensions.

The paper is organised as follows. Section 2 describes the kinematic model of an overconstrained planar *CDPR* with 4 cables. Section 3 provides the *FD* formulation and the derivation of its sensitivity to an error in one cable tension. The *WS* computation is shown in Section 4 as an application example. In Section 5 preliminary experimental results for the control of a prototype are reported. Finally, results of simulations and experiments are discussed.

## 2 Kinematic model

An *overconstrained planar CDPR* consists of a moving platform driven by  $n$  actuated cables, with  $n$  greater than the *EE DoFs*, i.e. 3. The degree of redundancy can be defined as  $\mu = n - 3$ . In this paper,  $n = 4$  and  $\mu = 1$ . Moreover, cables are considered massless and inextensible, and modeled as the line segments between the anchor points on the platform and the ones on the fixed base ( $A_i$  and  $B_i$  respectively, for  $i = 1, \dots, n$ , as in Fig. 1). An inertial frame  $Oxy$  and a mobile frame  $Px'y'$ , attached to the platform center of mass  $P$ , are introduced. Points  $P$ ,  $A_i$  and  $B_i$  are described by vectors  $\mathbf{p}$ ,  $\mathbf{a}_i$  and  $\mathbf{b}_i$  with respect to the inertial frame, whereas they are identified by  $\mathbf{p}'$ ,  $\mathbf{a}'_i$  and  $\mathbf{b}'_i$  in the mobile frame. The orientation of the platform is described by the

Fig. 1: Geometry of the  $i$ -th constraint of a planar CDPR.

rotation matrix  $\mathbf{R}(\theta)$ . The  $i$ -th cable vector is:

$$\boldsymbol{\rho}_i = \mathbf{a}_i - \mathbf{b}_i = \mathbf{p} + \mathbf{R}(\theta)\mathbf{a}'_i - \mathbf{b}_i, \quad \mathbf{R}(\theta) \triangleq \begin{bmatrix} \cos(\theta) & -\sin(\theta) \\ \sin(\theta) & \cos(\theta) \end{bmatrix} \quad (1)$$

If the pose  $[\mathbf{p}^T, \theta]^T$  of the platform is assigned, the  $i$ -th cable length  $l_i$  can be determined from the constraint imposed by the  $i$ -th cable:

$$\boldsymbol{\rho}_i^T \boldsymbol{\rho}_i - l_i^2 = 0 \quad (2)$$

The unit vector of the  $i$ -th cable, pointing from the base towards the platform, is:

$$\mathbf{t}_i = \frac{\boldsymbol{\rho}_i}{l_i} \quad (3)$$

### 3 Force-distribution sensitivity

The static equilibrium of the platform can be formulated as:

$$\mathbf{J}^T \boldsymbol{\tau} - \mathbf{W} = \mathbf{0} \quad (4)$$

where  $\mathbf{J}^T \in \mathbb{R}^{3 \times 4}$ , referred to as *structure matrix*, is the transpose of the Jacobian matrix of the inverse kinematics [13], whose  $i$ -th row is:

$$\mathbf{J}_i = [\mathbf{t}_i^T \quad -\mathbf{t}_i^T \mathbf{E} \mathbf{R} \mathbf{a}'_i], \quad \mathbf{E} \triangleq \begin{bmatrix} 0 & -1 \\ 1 & 0 \end{bmatrix} \quad (5)$$

$\boldsymbol{\tau} \in \mathbb{R}^4$  is the array of cable tensions, and  $\mathbf{W} = mg [0 \ 1 \ 0]^T \in \mathbb{R}^3$  is the external wrench if only gravity is acting on the system ( $m$  is the EE mass and  $g = -9.81 \text{ m/s}^2$ ).

For an OCDPR, if cable elasticity is not taken into account, the inverse static problem is underdetermined, due to actuation redundancy [14], thus it admits infinite solutions in the cable tensions. This problem is known in the literature as Force or Tension Distribution (FD) computation. The FD problem can be solved by different approaches, carefully analysed and compared in [15], depending on application

requirements. In general, for cables to remain taut, while the *EE* moves along a prescribed trajectory, an acceptable *FD* must be determined for each pose.

To derive the cable-tension sensitivity index, suitable partitions of the structure matrix and the tension array are introduced into the static equation (4). These partitions are based on the assumption that one cable, whose tension is called  $\tau_c$ , can be force-controlled, whereas the tensions of the remaining cables,  $\tau_d$ , depend on  $\tau_c$  and the external wrench  $\mathbf{W}$ . If we assume, for the time being, that the 4th cable is force-controlled, the array  $\boldsymbol{\tau}$  of cable tensions is:

$$\boldsymbol{\tau} \triangleq \begin{bmatrix} \tau_d \\ \tau_c \end{bmatrix} = \begin{bmatrix} \boldsymbol{\tau}_0 + \Delta\boldsymbol{\tau} \\ \tau_c \end{bmatrix} \quad (6)$$

and the structure matrix can be partitioned as:

$$\mathbf{J}^T = [\mathbf{J}_d \ \mathbf{J}_c] \quad (7)$$

where  $\mathbf{J}_d \in \mathbb{R}^{3 \times 3}$  and  $\mathbf{J}_c \in \mathbb{R}^3$ . Introducing definitions (6) and (7) in Eq. (4) yields:

$$\mathbf{W} = \mathbf{J}^T \boldsymbol{\tau} = [\mathbf{J}_d \ \mathbf{J}_c] \begin{bmatrix} \boldsymbol{\tau}_0 + \Delta\boldsymbol{\tau} \\ \tau_c \end{bmatrix} = \mathbf{J}_d(\boldsymbol{\tau}_0 + \Delta\boldsymbol{\tau}) + \tau_c \mathbf{J}_c \quad (8)$$

If  $\mathbf{J}_d$  is invertible (which is true if the *EE* is not in a geometrically singular configuration),  $\boldsymbol{\tau}_0$  is defined as the solution of Eq. (8) when  $\tau_c = 0$  and  $\Delta\boldsymbol{\tau} = \mathbf{0}$ :

$$\boldsymbol{\tau}_0 \triangleq \mathbf{J}_d^{-1} \mathbf{W} \quad (9)$$

The expression of  $\Delta\boldsymbol{\tau}$  is deduced from Eq. (8), by considering Eq. (9):

$$\Delta\boldsymbol{\tau} = -\tau_c \mathbf{J}_d^{-1} \mathbf{J}_c \quad (10)$$

Following the geometrical approach proposed in (7), the force distribution  $\boldsymbol{\tau}$  in Eq. (6) can be divided into two terms:  $\boldsymbol{\tau}_{ls}$ , obtained from the solution of the linear system (9), and  $\boldsymbol{\tau}_{ker}$ , which provides a variation of the overall distribution that still satisfies the *EE* equilibrium (4):

$$\boldsymbol{\tau} = \boldsymbol{\tau}_{ls} + \boldsymbol{\tau}_{ker} \quad (11)$$

With the definition given in Eq. (6), the first contribution is expressed as:

$$\boldsymbol{\tau}_{ls} = \begin{bmatrix} \boldsymbol{\tau}_0 \\ 0 \end{bmatrix} = \begin{bmatrix} \mathbf{J}_d^{-1} \mathbf{W} \\ 0 \end{bmatrix} \quad (12)$$

while the contribution  $\boldsymbol{\tau}_{ker}$  can be written as:

$$\boldsymbol{\tau}_{ker} = \begin{bmatrix} \Delta\boldsymbol{\tau} \\ \tau_c \end{bmatrix} = \tau_c \begin{bmatrix} -\mathbf{J}_d^{-1} \mathbf{J}_c \\ 1 \end{bmatrix} = \tau_c \mathbf{J}^\perp, \quad \mathbf{J}^\perp \triangleq \begin{bmatrix} -\mathbf{J}_d^{-1} \mathbf{J}_c \\ 1 \end{bmatrix} \quad (13)$$

$\mathbf{J}^\perp \in \mathbb{R}^4$  is the right nullspace of the  $(3 \times 4)$  matrix  $\mathbf{J}^T$ , namely the 4-dimensional vector such that  $\mathbf{J}^T \mathbf{J}^\perp = \mathbf{0}_{3 \times 1}$ . Indeed:

$$\mathbf{J}^T \mathbf{J}^\perp = [\mathbf{J}_d \ \mathbf{J}_c] \begin{bmatrix} -\mathbf{J}_d^{-1} \mathbf{J}_c \\ 1 \end{bmatrix} = -\mathbf{J}_c + \mathbf{J}_c = \mathbf{0} \quad (14)$$

The introduction of Eqs. (12) and (13) in Eq. (11) yields:

$$\boldsymbol{\tau} = \begin{bmatrix} \mathbf{J}_d^{-1} \mathbf{W} \\ 0 \end{bmatrix} + \tau_c \begin{bmatrix} -\mathbf{J}_d^{-1} \mathbf{J}_c \\ 1 \end{bmatrix} = \begin{bmatrix} \mathbf{J}_d^{-1} (\mathbf{W} - \tau_c \mathbf{J}_c) \\ \tau_c \end{bmatrix} \quad (15)$$

So, a *FD* can be determined by choosing a value of  $\tau_c \in \mathbb{R}$  and substituting it back in the first three elements at the right-hand side of Eq. (15), in order to compute the remaining three tensions:

$$\boldsymbol{\tau}_d = \boldsymbol{\tau}_0 + \Delta \boldsymbol{\tau} = \mathbf{J}_d^{-1} (\mathbf{W} - \tau_c \mathbf{J}_c) \quad (16)$$

It can be noticed from Eq. (13) that the right nullspace  $\mathbf{J}^\perp$  of the structure matrix  $\mathbf{J}^T$  represents the *force-distribution sensitivity*  $\boldsymbol{\sigma}$ . Namely,  $\boldsymbol{\sigma}$  shows how the overall cable tensions vary due to a unit change in the tension of the force-controlled cable:

$$\boldsymbol{\sigma} = \boldsymbol{\tau}_{ker}|_{\tau_c=1} = \begin{bmatrix} \sigma_1 \\ \sigma_2 \\ \sigma_3 \\ \sigma_4 \end{bmatrix} \triangleq \tau_c \mathbf{J}^\perp|_{\tau_c=1} = \mathbf{J}^\perp = \begin{bmatrix} -\mathbf{J}_d^{-1} \mathbf{J}_c \\ 1 \end{bmatrix} \quad (17)$$

A value  $|\sigma_i| > 1$  (resp.  $|\sigma_i| < 1$ ) in Eq. (17) means that the tension in cable  $i$  varies more (resp. less) than the tension in the 4th cable. Thus, if the cable with the largest  $|\sigma_i|$  is (locally) chosen to be force controlled, all other cables are guaranteed to have smaller tension errors than the error committed in the control of that cable. The largest component (in magnitude) of  $\boldsymbol{\sigma}$  is denoted  $\sigma_{i^*}$  and the corresponding cable,  $i^*$ . As a matter of fact, the preliminary choice of  $\tau_c$  as the tension of the 4th cable is irrelevant: the choice of another cable would change the numerical value of  $\boldsymbol{\sigma}$  but, thanks to the linear nature of the problem, the cable with the highest sensitivity to tension variations would remain the same.

As a result, it is possible to compute  $\boldsymbol{\sigma}$  in advance, along with the *WS*, so that, for every *EE* pose, the cable with highest sensitivity can be selected to be force-controlled.

## 4 Workspace characterization

As an example of application of the *FD* sensitivity, the constant-orientation wrench-feasible *WS* of a planar *OCDPRs* with two different cable arrangements is presented in this section, and the highest-sensitivity cable  $i^*$  is determined in each *WS* configuration. A kernel-based approach is used for the *WS* calculation [13], where the nullspace (or kernel)  $\mathbf{J}^\perp$  is computed as in Eq. (17).

The wrench-feasible *WS* is defined as the set of poses  $[\mathbf{p}^T, \theta]^T$  for which:

$$\exists \boldsymbol{\tau} : \quad \mathbf{T}_{min} \leq \boldsymbol{\tau} \leq \mathbf{T}_{max}, \quad \mathbf{J}^T \boldsymbol{\tau} - \mathbf{W} = \mathbf{0} \quad (18)$$

where all elements of the arrays  $\mathbf{T}_{min}$  and  $\mathbf{T}_{max} \in \mathbb{R}^4$  are equal to the tension limits  $\tau_{min}$  and  $\tau_{max}$ , respectively. Considering the partition (6), Eq. (18) can be written as:

$$\tau_{min} \leq \tau_c \leq \tau_{max} \quad (19)$$

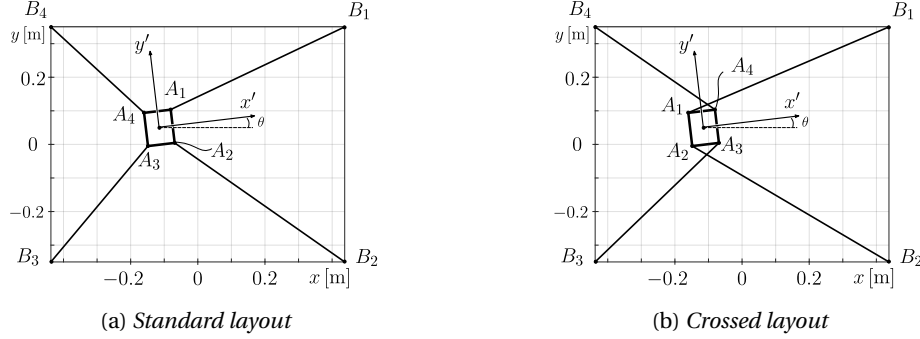


Fig. 2: Cable arrangements of the planar 4-cable OCDPR.

$$\boldsymbol{\tau}_{min} \leq \boldsymbol{\tau}_d \leq \boldsymbol{\tau}_{max}, \quad \boldsymbol{\tau}_{min}, \boldsymbol{\tau}_{max} \in \mathbb{R}^3 \quad (20)$$

Due to Eq. (16), Eq. (20) yields:

$$\boldsymbol{\tau}_{min} \leq \mathbf{J}_d^{-1}(\mathbf{W} - \tau_c \mathbf{J}_c) \leq \boldsymbol{\tau}_{max} \quad (21)$$

$$-\boldsymbol{\tau}_{max} + \mathbf{J}_d^{-1}\mathbf{W} \leq \tau_c \mathbf{J}_d^{-1}\mathbf{J}_c \leq -\boldsymbol{\tau}_{min} + \mathbf{J}_d^{-1}\mathbf{W} \quad (22)$$

$$\mathbf{a} \leq \tau_c \mathbf{c} \leq \mathbf{b}, \quad \mathbf{a} \triangleq -\boldsymbol{\tau}_{max} + \mathbf{J}_d^{-1}\mathbf{W}, \quad \mathbf{b} \triangleq -\boldsymbol{\tau}_{min} + \mathbf{J}_d^{-1}\mathbf{W}, \quad \mathbf{c} \triangleq \mathbf{J}_d^{-1}\mathbf{J}_c \quad (23)$$

$$\begin{bmatrix} a_1 \\ a_2 \\ a_3 \end{bmatrix} \leq \tau_c \begin{bmatrix} c_1 \\ c_2 \\ c_3 \end{bmatrix} \leq \begin{bmatrix} b_1 \\ b_2 \\ b_3 \end{bmatrix} \quad (24)$$

Thus, if the intersection between the four inequalities in Eq. (19) and (24) is nonempty, there is at least one value of  $\tau_c$  for which a feasible  $FD$  exists, for a given  $EE$  pose.

By using the above method, the wrench-feasible constant-orientation  $WS$  of a planar 3-DoF 4-cable  $CDPR$  model may be computed and characterized by the variation of  $i^*$  throughout it. In case of planar  $CDPR$ s, the constant-orientation  $WS$  can be easily visualized in 2D, and represented with a regular discrete grid of  $N \times M$  points. In the following example,  $N = M = 100$ . Moreover,  $m = 2.5$  kg,  $\tau_{min} = 10$  N, and  $\tau_{max} = 80$  N.

The  $CDPR$  at hand (Fig. 2) has rectangular base ( $0.875$  m  $\times$   $0.700$  m) and mobile platform ( $0.080$  m  $\times$   $0.100$  m). The inertial frame  $Oxy$  is located in center of the base and the moving frame  $Px'y'$  at the center of the  $EE$ , coinciding with its center of mass. Two different cable arrangements are considered on the same model: a *standard* layout (Fig. 2a), where each cable goes from one vertex of the rectangular base to the corresponding vertex of the  $EE$ , and a *crossed* layout (Fig. 2b), where cables cross under and above the platform.

The wrench-feasible  $WS$  with constant orientation  $\theta = 0^\circ$  is shown in Fig. 3 for the *standard* (Fig. 3a) and the *crossed* layout (Fig. 3b). Four distinct constant- $i^*$  areas emerge from the  $FD$  sensitivity analysis: the change in  $i^*$  occurs exactly when the  $EE$  position crosses one coordinated axis of the inertial frame  $Oxy$ . For the *standard*



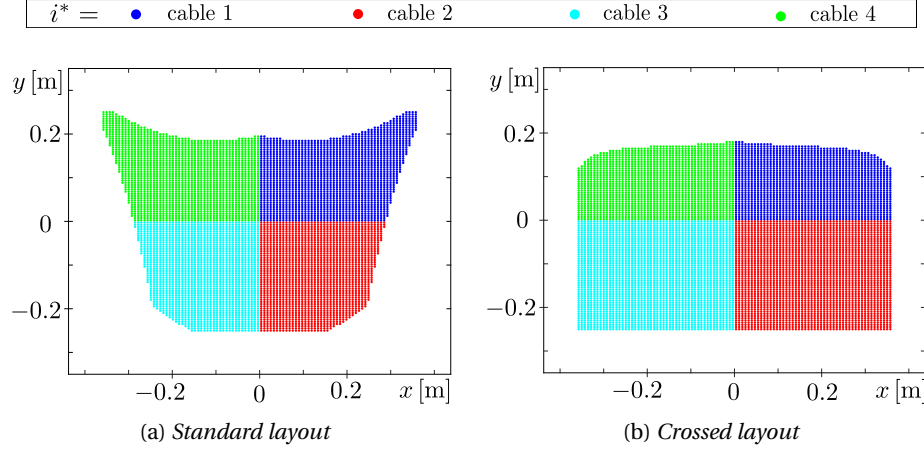


Fig. 3: Highest-sensitivity cable ( $i^*$ ) on the wrench-feasible WS of the planar 4-cable OCDPR with constant orientation  $\theta = 0^\circ$ .

layout, only the case with  $\theta = 0^\circ$  is analysed, since this cable configuration has a very limited orientation capability, as reported in [16]. For the *crossed* layout, four other different cases are investigated. The WS for constant orientations  $\theta = \pm 10^\circ$  is shown in Figs. 4a and 4b. It can be noticed that, one sensitivity area, respectively for  $i^* = 3$  when  $\theta = 10^\circ$  (Fig. 4a), and  $i^* = 2$  when  $\theta = -10^\circ$  (Fig. 4b), is significantly larger, compared to the case  $\theta = 0^\circ$  in Fig. 3b. Also, the dimensions of this area increase for larger values of  $\theta$ , as shown in Figs. 4c and 4d.

Due to space limitations, the detailed analysis of  $FD$  sensitivity values  $\sigma_i$  throughout the WS is not reported. However, simulation results show that, for all configurations near transition borders, the values of  $\sigma_i$  in contiguous areas are very similar. On the other hand, at the edges of the WS, far from transitions, those values significantly differ. For example, in the bottom left corner of the crossed-layout WS in Fig. 3b,  $|\sigma_3|$  is ten times greater than  $|\sigma_4|$ . As a consequence, for close-to-transition configurations, it may not be worth changing the force-controlled cable, but it may be beneficial near WS edges.

Two facts are noteworthy: (i) the sensitivity areas for negative angles are symmetrical with respect to those for positive angles, and (ii) when  $\theta \neq 0^\circ$  the boundaries of the regions where  $i^*$  is constant are not straight lines. These observations are relevant if a hybrid-input control strategy is implemented on the manipulator, as proposed in [10, 11]. According to this strategy, three cables are length-controlled, while the remaining one is force-controlled. As introduced in Sec. 3, cable  $i^*$  can be chosen to be force-controlled, since its tension-control error causes the smallest tension errors in the other cables in a given configuration. On the other hand, while the  $EE$  performs a prescribed trajectory inside the WS, the force-controlled cable should change when crossing from one sensitivity area to another. Changing the control input type (length or force) could cause a discontinuity of the control action,

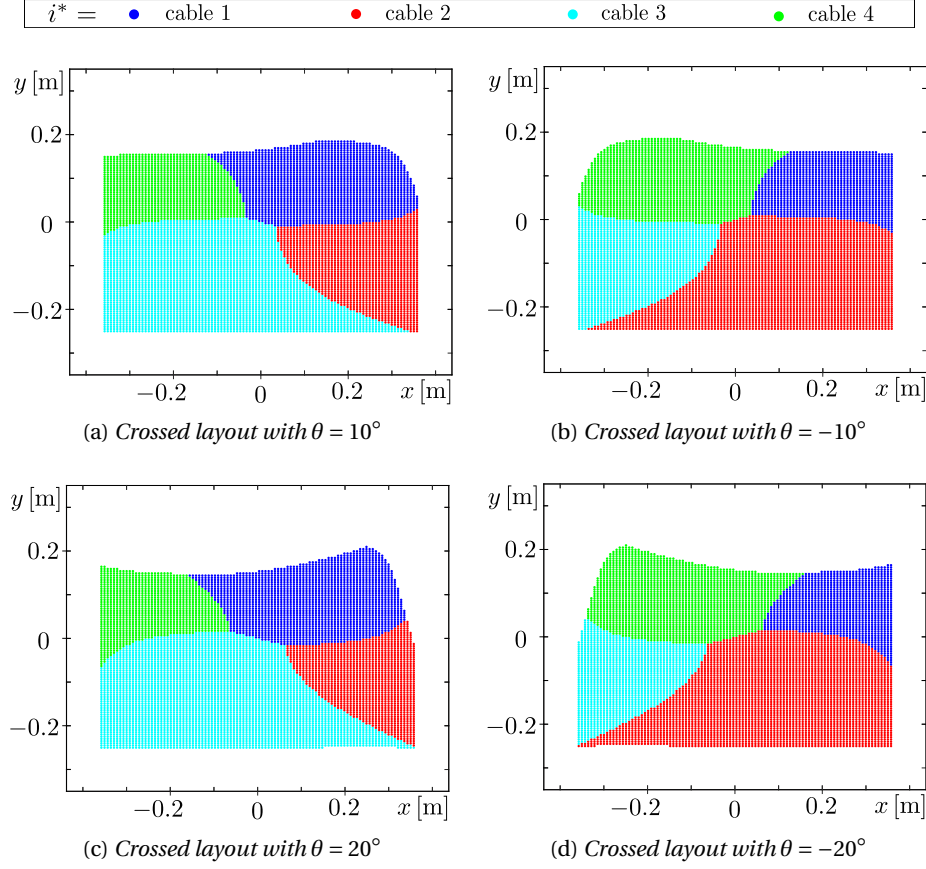


Fig. 4: *Highest-sensitivity cable ( $i^*$ ) on the wrench-feasible WS of the planar 4-cable OCDPR with variable constant orientation  $\theta = 10^\circ, -10^\circ, 20^\circ$  and  $-20^\circ$ .*

since the error tracked by the controller changes. Thus, it can be beneficial to reduce the number of constant- $i^*$  boundary transitions during motion. To do so, an area with constant  $i^*$  can be enlarged, in order to perform an entire trajectory without crossing such boundaries. For this purpose:

1. for a given robot design, the platform orientation can be varied, unless  $\theta = \text{const}$  is prescribed by the application;
2. the positions of cable anchor points on the *EE* can be optimized in order to maximize one sensitivity area so that it includes the entire *WS* needed by the application at hand.

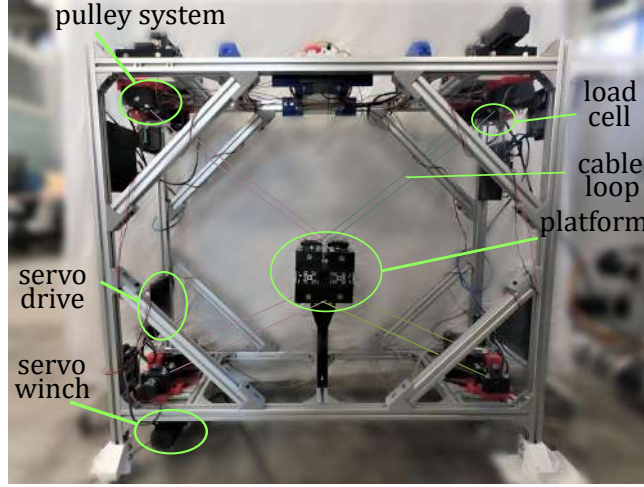


Fig. 5: Planar 3-DoF 4-cable OCDPR prototype developed at IRMA L@B.

## 5 Experiments on hybrid-input control

In this section, a hybrid-input control strategy is preliminarily investigated, and applied to a planar 3-DoF 4-cable OCDPR prototype developed at IRMA L@B (Fig. 5): this prototype has to perform quasi-static non-contact tasks, such as laser engraving or laser cutting. The prototype presents a *crossed* cable layout, as in Fig. 2b, and its geometrical parameters are those given in Sec. 4. Four self-manufactured servo winches are fixed to the corners of an aluminium-profile base and each one of them drives a cable coiled in a loop onto the pulley system. The high-level robot controller runs on a *Real-Time Linux* PC at 1 kHz rate. When a trajectory in the Cartesian space is assigned, the controller computes the feedforward hybrid inputs for the robot actuators. The servo-winch control schemes are also developed in house and run on a *ST Nucleo-H743ZI* development board at 10 kHz. In addition to controlling the motor angle, this allows us to directly feed a cable-tension command to the drive, to compare said command with the signal of a load-cell embedded in the cable transmission, and regulate the tension by a *PID* controller at drive level.

The hybrid-input control strategy requires that three cables, equal to the number of platform *DoFs*, are length-controlled while the redundant cable is force-controlled. The rationale behind this choice is that three length-controlled cables are sufficient for precisely controlling the pose of the planar *EE*, whereas the 4th cable is needed to keep the remaining cables under tension. Cable  $i^*$  is chosen to be force-controlled, since errors in its tension estimation (or low-level feedback control) limitedly impact the overall *FD*.

Two experiments are conducted, while the *EE* follows the same circular trajectory with a constant linear speed of 1 cm/s, with  $\theta = 0^\circ$ , that is:

$$\mathbf{p}(t) = \begin{bmatrix} x \\ y \end{bmatrix} = \begin{bmatrix} P_{0x} + r \cos\left(\frac{2\pi t}{T}\right) \\ P_{0y} + r \sin\left(\frac{2\pi t}{T}\right) \end{bmatrix}, \quad \begin{matrix} P_{0x} = -0.06 \text{ m}, P_{0y} = -0.06 \text{ m} \\ r = 0.05 \text{ m}, T = 31.4 \text{ s} \end{matrix} \quad (25)$$

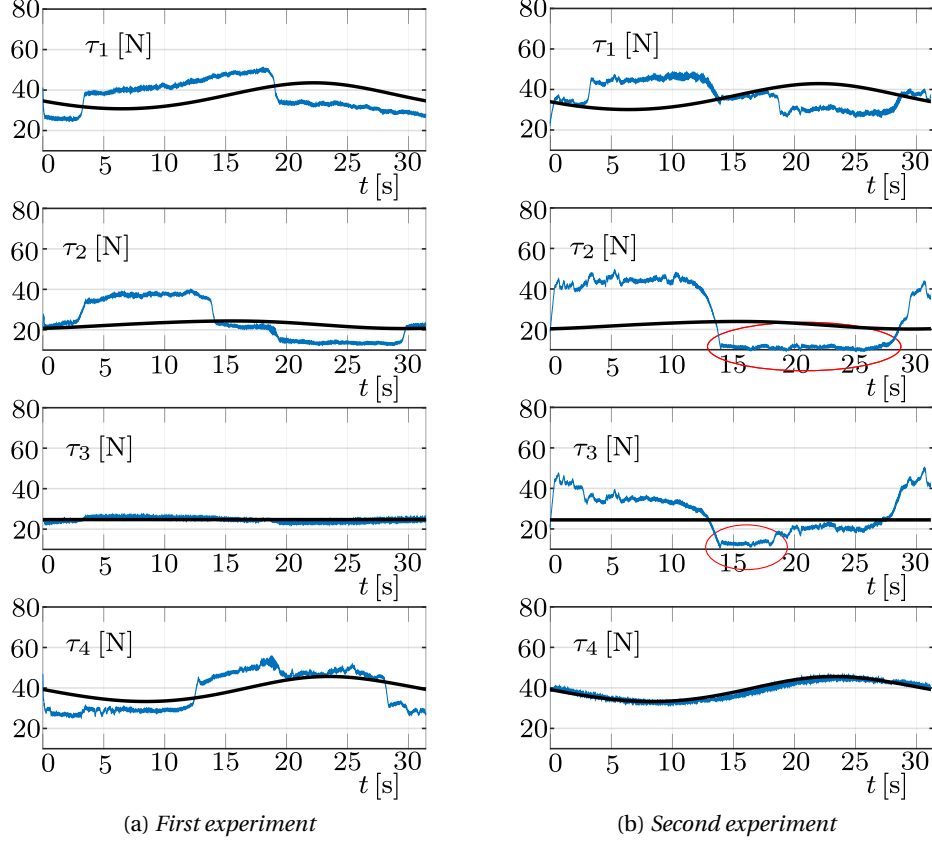


Fig. 6: Real (blue) and computed (black) FD during experiments.

The value of the constant speed is selected so that a piece of paper may be cut with a 2.5 W laser-diode mounted onto the *EE*. The whole trajectory lies in the area where  $i^* = 3$  in Fig 3b. The *FD* over the whole trajectory is calculated, by choosing  $\tau_c = 25$  N as a constant value and considering gravity as the only external wrench. In the first experiment, the 3rd cable, whose tension errors influence the *FD* as little as possible, is force controlled, so that  $\tau_3 = \tau_c$ . In the second experiment, the 4th cable, whose tension errors more influence the *FD*, is force controlled. The tension set-points of the tension-controlled cable are chosen so that the same theoretical *FD* is generated in both experiments.

Experimental results on the actual *FD* attained during the trajectory execution are shown in Fig. 6. It can be noticed that the low-level force controller is effective in maintaining the controlled cable tension very close to the assigned value, but the other cable tensions are quite distant from their theoretical value, which is compatible with the oversimplified model that was adopted and the cheap robot

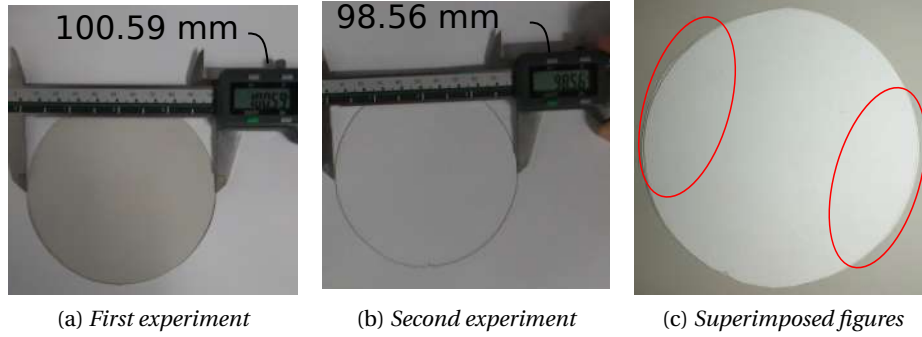


Fig. 7: Results of the laser-cutting operation.

components (most of them are plastic made). However, when the 3rd cable is force-controlled during the first experiment, the other tensions, as measured by the load cells, never fall below the lower cable tension limit  $\tau_{min} = 10$  N. Conversely, during the second experiment, when the 4th cable is force-controlled, there is a prolonged period for which the second and third cables are practically slack (see the red-circled areas in Fig. 6b). In practice, by force-controlling the highest-sensitivity cable ( $i^*$ ), the *FD* errors with respect to the theoretical ones are minimized.

The paper-cutting operation confirms that the first experiment produced good results also in practice, while the results of the second experiments are poorer (see Fig. 7). Figure 7a shows a well-cut circle executed with millimetric accuracy, whereas the second experiment produced a more elliptic shape (without managing to complete the cut), as shown in Fig. 7b. The hybrid-input control strategy, where cable  $i^*$  is force-controlled, produced good preliminary results, despite the hardware limitations.

## 6 Conclusions

In this paper, the *FD* sensitivity to tension errors in one cable was investigated, and the cable whose tension error plays the least influence was analytically derived. The wrench-feasible *WS* of a 3-*DoF* planar *OCDPR* with 4-cables was calculated with two different cable arrangements, and the areas where different cables have the highest sensitivity were displayed. A hybrid-input control strategy was preliminarily investigated on a prototype, with one cable being force-controlled and the others being length-controlled. The force control of the highest-sensitivity cable showed promising results. This strategy is a simpler alternative to well known cascade position/force control strategies, and provides a good motion accuracy while maintaining all cables taut. In the future, we will expand the concept of *FD* sensitivity to *OCDPRs* with degree of redundancy greater than one, and we will characterize the stability of the hybrid-input controller in case the force controlled cable is changed during a trajectory.

## References

1. T. Bruckmann, W. Lalo, K. Nguyen, and B. Salah, "Development of a storage retrieval machine for high racks using a wire robot," in *ASME 2012 Int. Design Engineering Technical Conferences*, Chicago, USA, 2012, pp. 771–780.
2. T. Bruckmann, H. Mattern, A. Spengler, C. Reichert, A. Malkwitz, and M. König, "Automated construction of masonry buildings using cable-driven parallel robots," in *33rd Int. Symposium on Automation and Robotics in Construction*, Auburn, USA, 2016, pp. 332–340.
3. J.-B. Izard, A. Dubor, P.-E. Hervé, E. Cabay, D. Culla, M. Rodriguez, and M. Barrado, "Large-scale 3D printing with cable-driven parallel robots," *Construction Robotics*, vol. 1, no. 1, pp. 69–76, 2017.
4. S. Kawamura, W. Choe, S. Tanaka, and H. Kino, "Development of an ultrahigh speed robot FALCON using parallel wire drive systems," *J. of the Robotics Society of Japan*, vol. 15, no. 1, pp. 82–89, 1997.
5. S. Bouchard, C. Gosselin, and B. Moore, "On the ability of a cable-driven robot to generate a prescribed set of wrenches," *J. Mechanisms Robotics*, vol. 2, no. 1, 2010.
6. C. Gosselin and M. Grenier, "On the determination of the force distribution in overconstrained cable-driven parallel mechanisms," *Meccanica*, vol. 46, no. 1, pp. 3–15, 2011.
7. T. Bruckmann, A. Pott, and M. Hiller, "Calculating force distributions for redundantly actuated tendon-based stewart platforms," in *Advances in Robot Kinematics*, J. Lenarčič and B. Roth, Eds. Springer, 2006, pp. 403–412.
8. J. Lamaury and M. Gouttefarde, "A tension distribution method with improved computational efficiency," in *Cable-Driven Parallel Robots*, T. Bruckmann and A. Pott, Eds. Springer, 2013, pp. 71–85.
9. A. Pott, "An improved force distribution algorithm for over-constrained cable-driven parallel robots," in *Computational Kinematics*, F. Thomas and A. Perez Gracia, Eds. Springer, 2014, pp. 139–146.
10. S. Bouchard and C. Gosselin, "A simple control strategy for overconstrained parallel cable mechanisms," in *Proc. of the 20th Canadian Congress of Applied Mechanics (CANCAM 2005)*, Montreal, Quebec, Canada, 2005.
11. T. Bruckmann, L. Mikelsons, M. Hiller, and D. Schramm, "A new force calculation algorithm for tendon-based parallel manipulators," in *2007 IEEE/ASME int. conf. on advanced intelligent mechatronics*, Zurich, Switzerland, 2007, pp. 1–6.
12. W. Kraus, V. Schmidt, P. Rajendra, and A. Pott, "System identification and cable force control for a cable-driven parallel robot with industrial servo drives," in *2014 IEEE Int. Conf. on Robotics and Automation (ICRA)*, Hong Kong, China, 2014, pp. 5921–5926.
13. R. Verhoeven, M. Hiller, and S. Tadokoro, "Workspace, stiffness, singularities and classification of tendon-driven stewart platforms," in *Advances in robot kinematics: Analysis and Control*, J. Lenarčič and M. L. Husty, Eds. Springer, 1998, pp. 105–114.
14. J.-P. Merlet, "Wire-driven parallel robot: open issues," in *Romansy 19–Robot Design, Dynamics and Control*, V. Padois, P. Bidaud, and O. Khatib, Eds. Springer, 2013, pp. 3–10.
15. A. Pott, *Cable-driven Parallel Robots: Theory and Application*, B. Siciliano and O. Khatib, Eds. Springer, 2018.
16. M. Gouttefarde, S. Krut, O. Company, F. Pierrot, and N. Ramdani, "On the design of fully constrained parallel cable-driven robots," in *Advances in Robot Kinematics: Analysis and Design*, J. Lenarčič and P. Wenger, Eds. Springer, 2008, pp. 71–78.